






# Real-time Nonlinear Model Predictive Control (NMPC) Strategies using Physics-Based Models for Advanced Lithium-ion Battery Management System (BMS)

Suryanarayana Kolluri,<sup>1,2</sup>  Sai Varun Aduru,<sup>2</sup> Manan Pathak,<sup>2</sup> Richard D. Braatz,<sup>3,\*</sup>   
and Venkat R. Subramanian<sup>1,2,\*\*,z</sup> 

<sup>1</sup>Walker Department of Mechanical Engineering & Material Science Engineering, Texas Materials Institute, The University of Texas at Austin, Austin, Texas 78712, United States of America

<sup>2</sup>BattGenie Inc., Seattle, Washington 98105, United States of America

<sup>3</sup>Massachusetts Institute of Technology, Cambridge, Massachusetts 02139, United States of America

Optimal operation of lithium-ion batteries requires robust battery models for advanced battery management systems (ABMS). A nonlinear model predictive control strategy is proposed that directly employs the pseudo-two-dimensional (P2D) model for making predictions. Using robust and efficient model simulation algorithms developed previously, the computational time of the nonlinear model predictive control algorithm is quantified, and the ability to use such models for nonlinear model predictive control for ABMS is established.

© 2020 The Author(s). Published on behalf of The Electrochemical Society by IOP Publishing Limited. This is an open access article distributed under the terms of the Creative Commons Attribution 4.0 License (CC BY, <http://creativecommons.org/licenses/by/4.0/>), which permits unrestricted reuse of the work in any medium, provided the original work is properly cited. [DOI: 10.1149/1945-7111/ab7bd7]



Manuscript submitted September 30, 2019; revised manuscript received January 31, 2020. Published April 6, 2020. *This was paper 106 presented at the Dallas, Texas, Meeting of the Society, May 26–May 30, 2019.*

## List of variables for P2D model

$c$	Electrolyte concentration
$c^s$	Solid Phase Concentration
$D$	Liquid phase Diffusion coefficient
$D_{eff}$	Effective Diffusion coefficient
$D^s$	Solid phase diffusion coefficient
$E_a$	Activation Energy
$F$	Faraday's Constant
$I_{app}$	Applied Current
$j$	Pore wall flux
$k$	Reaction rate constant
$l$	Length of region
$R$	Particle Radius, or Residual
$t_+$	Transference number
$\tau$	Time, Temperature
$U$	Open Circuit Potential
$W$	Weight Function
$\varepsilon$	Porosity
$\varepsilon_f$	Filling fraction
$\theta$	State of Charge
$\kappa$	Liquid phase conductivity
$\sigma$	Solid Phase Conductivity
$\Phi_1$	Solid Phase Potential
$\Phi_2$	Liquid Phase Potential
$k_c$	Proportional Gain
$\tau_i$	Integral Time Constant

## List of subscripts

$f$	Final, as for final time
$k$	Represents the time instant
$LB$	Lower Bound
$UB$	Upper Bound
$app$	Applied
$eff$	Effective, as for diffusivity or conductivity
$c$	Related to the electrolyte concentration

$c^s$	Related to solid-phase concentration
$n$	Related to the negative electrode—the anode
$p$	Related to the positive electrode—the cathode
$s$	Related to the separator

## List of superscripts

$T$	Transpose
$max$	Maximum
$Set$	Setpoint
$avg$	Average, as for solid-phase concentration
$surf$	Surface, as for solid-phase concentration
$s$	Related to solid-phase
1	Related to the solid-phase potential
2	Related to the liquid-phase potential

Lithium-ion batteries are now ubiquitous in applications ranging from cellphones, laptops, electric vehicles, and even electric flights. Safety and long recharging times along with capacity and power fade remain some of the major concerns for lithium-ion batteries. Advanced battery management systems (ABMS) that can counter these issues and implement optimal usage patterns are critical for efficient use of batteries. Various optimal charging strategies have been proposed by researchers in recent times that minimize battery degradation or charge the batteries faster.<sup>1–4</sup> However, most of these strategies have been derived either using reduced-order physics-based models, or implemented as open-loop control profiles based on offline calculations. While model order-reduction simplifies the governing model and decreases the numerical stiffness of the underlying full model, it often comes at the cost of simplification of actual physics of the system. Additionally, lithium-ion battery models have uncertainties due to low confidence in estimated system parameters, or parameters that can change with time, which makes open-loop control strategy less effective and necessitates a closed-loop (feedback) control for optimal system performance.

Model predictive control (MPC) is an advanced closed-loop control strategy, which due to its characteristics, can be incorporated into ABMS to derive optimal charging protocols. This framework, while satisfying physical and operational constraints, evaluates the control objective based on the future predictions of the plant. Various MPC techniques deriving optimal charging profiles using

\*Electrochemical Society Member.

\*\*Electrochemical Society Fellow.

<sup>z</sup>E-mail: [venkat.subramanian@utexas.edu](mailto:venkat.subramanian@utexas.edu)

approximated porous electrode pseudo-2-dimensional (P2D) models have been published in the literature. Xavier et al. proposed MPC strategies for controlling lithium-ion batteries using equivalent circuit models.<sup>5</sup> Torchio et al. proposed a linear MPC strategy based on the input-output approximation of the P2D model.<sup>6</sup> Torchio et al. also proposed health-aware charging protocols for lithium ion batteries using a linear MPC algorithm along with piecewise linear approximation and linear time-varying MPC strategies for lithium-ion batteries.<sup>7,8</sup> Klein et al. proposed a nonlinear MPC framework based on a reduced-order P2D model.<sup>9</sup> Lee et al. proposed an MPC algorithm for optimal operation of an energy management system containing a solar photovoltaic panel and batteries connected to a local load in a microgrid.<sup>10</sup> Liu et al. derived nonlinear MPC profiles for optimal health of lithium ion batteries using a full single-particle model.<sup>11</sup> Traditionally, the high computational cost of online calculations has been often cited as one of the main reasons for not using detailed P2D models in MPC formulations.

While nonlinear MPC formulations based on battery models have been developed before, we propose implementation of such strategies using more robust and efficient numerical solvers along with reformulated models, allowing us to significantly reduce the computational time of this technique and enabling their use in real-time ABMS platforms. In this work, we design a nonlinear MPC controller capable of deriving optimal charging profiles using the detailed isothermal P2D model in real-time. The nonlinear model predictive control scheme is summarized in section 2, followed by a discussion on the numerical optimization approach used for solving the optimal control problem within the MPC framework. We then implement the nonlinear model predictive control technique to derive optimal charging protocols for the thin film nickel hydroxide electrode, discussed in section 3, for setpoint tracking objectives. Section 4 demonstrates the nonlinear model predictive controller designed by using the detailed reformulated P2D model. Section 5 analyses the effect of tuning parameters on the performance of the designed controller followed by a description of the computational efficiency achieved by the controller while using the detailed P2D model. Section 6 summarizes and outlines the future directions of the work.

### Nonlinear Model Predictive Control

Model Predictive Control (MPC) is a multivariable control strategy with an explicit constraint-handling mechanism. This strategy involves generating a sequence of manipulated inputs over a control horizon, which optimizes a defined control objective over a

prediction horizon, using an explicit process model.<sup>12,13</sup> If a nonlinear process model is used within the framework, then this strategy is termed as Nonlinear Model Predictive Control (NMPC).<sup>12,14</sup> A nonlinear optimal control formulation<sup>15</sup> related to the NMPC strategy given in literature is

**Formulation—I:**

$$\min J = \int_0^{T_f} \varphi(x(t), u(t), t) dt \quad [1]$$

Subject to:

$$\frac{dx(t)}{dt} = f(x(t), u(t), t)g(x(t), u(t), t) = 0 \quad [2]$$

$$u_{LB} \leq u(t) \leq u_{UB} \quad [3]$$

$$x_{LB} \leq x(t) \leq x_{UB} \quad [4]$$

- Equation 1 defines the control objective  $J$  with respect to a continuous-time model computed for a time horizon  $[0, T_f]$  over which the cost function  $\varphi$  is minimized.

- Equation 2 defines the equality constraints that describe the dynamics of the nonlinear plant denoted by a set of differential algebraic equations (DAEs), where functions  $f$  and  $g$  describe the differential and algebraic relations, respectively,  $x(t)$  represents the states of the plant, and  $u(t)$  represents the input signals to the plant.

- Equation 3 shows the bounds on the decision variables (input variables)  $u(t)$  for all  $t \in [0, T_f]$ , where  $u_{UB}$  denotes the upper bound and  $u_{LB}$  denotes the lower bound.

- Equation 4 represents the bounds on the state variables for all  $t \in [0, T_f]$  where  $x_{UB}$  denotes the upper bound and  $x_{LB}$  denotes the lower bound on the respective state variable.

The optimal control problem in Formulation I, defined by Eqs. 1–4 is a constrained dynamic optimization which can be solved using *direct* or *indirect* methods.<sup>15,16</sup> This work implements a *direct* method referred to as *sequential dynamic optimization*. The resulting nonlinear program (NLP) used in this method is discussed in the next subsection.

**NMPC optimal control problem using sequential dynamic optimization.**—In Formulation—I the decision variable  $u(t)$  of the

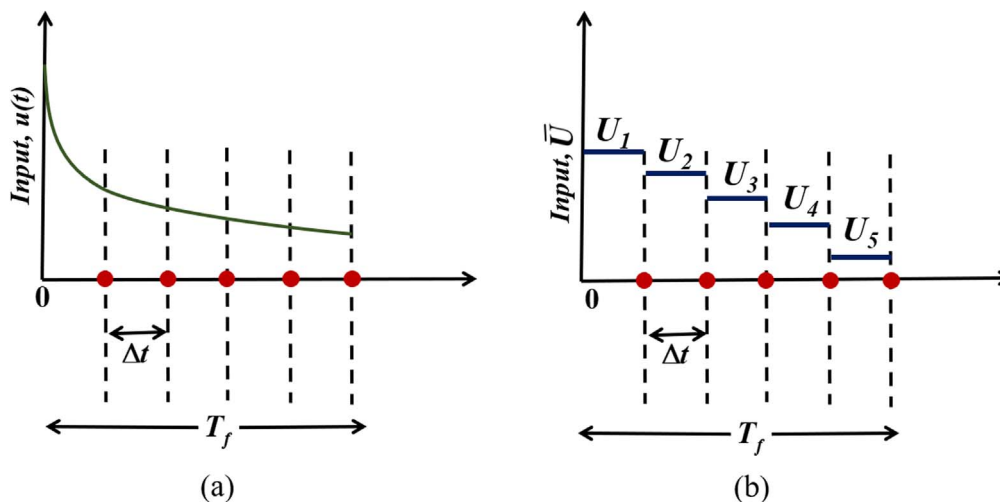


**Figure 1.** Converting the continuous decision variable to discrete decision variables in the sequential dynamic optimization method: (a) represents the continuous input variable  $u(t)$ , (b) represents the discrete input variable over the time window  $[0, T_f]$ .

**Table I. NMPC Algorithm.**

- Given:** Mathematical model  $f$ , initial condition  $x(0)$ , prediction horizon  $p$ , control horizon  $m$ , sampling time  $\Delta t$ , and weighting matrices  $Q$  and  $R$
- Step 1:** At the current sampling time  $t_k$ , set  $x(t_{k-1}) \leftarrow x(t_k)$
- Step 2:** Solve Formulation II for a sequence of  $m$  optimal input variables  $\{U(1), U(2), \dots, U(m)\}$
- Step 3:** Set  $u(t_k) \leftarrow U(1)$  and inject the input to the plant
- Step 4:** At the sampling time instant  $t_{k+1}$ , obtain the plant measurement  $y_m$
- Step 5:** Corresponding to  $y_m$ , estimate the states  $x^*(t_{k+1})$  (this work assumes full state feedback, for which all the states are measurable)
- Step 6:** Set  $t_k \leftarrow t_{k+1}$
- Step 7:** Shift the prediction horizon  $p$  forward and repeat Step 1

optimal control problem is a continuous variable as shown in Fig. 1a. In sequential dynamic optimization, the infinite-dimensional optimal control problem is reduced to a finite-dimensional NLP through discretization of the input signal  $u(t)$  to  $N$  discrete node points, where  $N$  is defined as the total time  $T_f$  over the sampling time  $\Delta t$  ( $N = \frac{T_f}{\Delta t}$ ).<sup>16</sup> In this method, the input signal  $u(t)$  is assumed to be a piecewise constant at each sampling time instant  $\Delta t$  as shown in Fig. 1b. To formulate the finite-dimensional NLP, the input signal is discretized as  $U \in \mathbb{R}^p$ , a  $p$ -dimensional real-valued vector, where  $p$  is the prediction horizon. The reformulated finite-dimensional NLP is

**Formulation—II:**

$$\min_{U_k} J(x(t), U_k) = \sum_{k=1}^p \varphi(x(t), U_k) \quad [5]$$

Subject to:

$$\begin{aligned} \frac{dx(t)}{dt} &= f(x(t), U_k) \\ g(x(t), U_k) &= 0, k = 1, \dots, p \end{aligned} \quad [6]$$

$$U_{j-1} = U_j, j = m + 1, \dots, p \quad [7]$$

$$u_{LB} \leq U_k \leq u_{UB}, k = 1, \dots, p \quad [8]$$

$$x_{LB} \leq x \leq x_{UB} \quad [9]$$

Equation 5 is the objective function, minimizing the cost function  $\varphi$ , which is solved for a finite number of optimal input signals, at

time instants  $t_k$  for  $k = 1, \dots, p$ . The cost function  $\varphi$  in Eq. 5 for the setpoint tracking objective is written in the discrete-time formulation as

$$\begin{aligned} \varphi &= \sum_{k=1}^p (v_k - v^{set})^T Q (v_k - v^{set}) \\ &+ \sum_{k=1}^m (U_k - U_{k-1})^T R (U_k - U_{k-1}) \end{aligned} \quad [10]$$

where  $v_k$  denotes the controlled variable at the time instant  $t_k$ ,  $v^{set}$  denotes its desired setpoint,  $U_k$  denotes the predicted optimal manipulated variable at the time instant  $t_k$ , and  $Q$  and  $R$  denote weighting parameters for setpoint tracking and input variations, respectively.

- Equation 6 are set of equality constraints imposed by the DAE model equations for specific time interval  $\Delta t$  where  $\Delta t \in [t_{k-1}, t_k]$  for  $k = 1, \dots, p$  instants.

- Equation 7 describes the control horizon  $m$ . This constraint implies that the input signal beyond the control horizon assumes a constant value until the end of the prediction horizon. This constant value is equal to the value of the input signal at the end of the control horizon ( $U_m$ ).

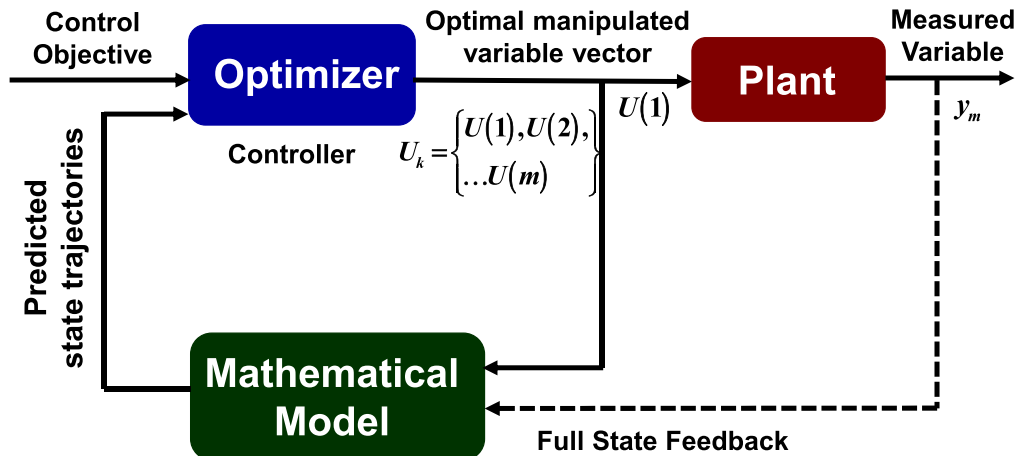
- Equation 8 describes the bounds on the input variables over the prediction horizon  $p$  where  $k = 1, \dots, p$ .

- Equation 9 describes the bounds on the state variables over the prediction horizon  $p$ .

Formulation II (Eqs. 5–9) can now be numerically solved using an optimizer along with a robust numerical integrator (DAE solver). In any optimal control problem within the NMPC framework, the optimizer is treated as an “outer-loop” and the DAE solver is treated as an “inner-loop.”

At each iteration in optimization, the vector of the decision variables  $U$  provided by the optimizer is fed to the DAE solver to simulate the model for a finite number of time instants. The state variable trajectories from the DAE solver are then used to evaluate the objective and constraint functions. These functional values are sent to the optimizer, which provides an updated vector of the decision variables for the next optimization calculation. The resulting sequence of simulation and optimization iterations is also referred to as *sequential simulation-optimization*.<sup>16</sup>

**Receding horizon approach.**—In the MPC framework, after obtaining the “ $p$ ” optimal inputs, the first optimal input is sent to the plant. The resulting feedback from the plant is incorporated by estimating the states to minimize the plant-model mismatch, upon which the resultant NLP is solved recursively at each sampling


**Figure 2.** Schematic representation of a model predictive controller.

instant. This recursive method is also termed as ‘receding horizon control’<sup>13</sup> which is described by the algorithm in Table I. A pictorial illustration the NMPC algorithm is shown in Fig. 2.

The design parameters for the NMPC formulation are, (i) prediction horizon  $p$ , (ii) control horizon  $m$  ( $m$  is specified so that  $m \leq p$ ), (iii) the sampling period  $\Delta t$ , and (iv) weighting parameters  $[Q, R]$  (in the objective function of Formulation II, Eq. 10) for setpoint tracking and input variations. The weighting parameter  $R$  makes the response of NMPC sluggish. In this work, it is taken as zero to enable fast charging strategy.

In real systems, it might not be possible to measure all the states of the system. In that case, the states corresponding to the new plant measurement at sampling instant  $t_{k+1}$  need to be estimated (Step 5 in Table I). In practice, nonlinear state estimators such as Extended Kalman Filter (EKF) or Moving Horizon Estimator (MHE) are used to estimate the states for the control algorithm. The use of these estimators is under investigation by the authors and will be reported in the future work. Here, the model is differentiated from the plant by introducing model uncertainty by perturbing certain parameters of the system, as described in the Appendix.

### Thin Film Nickel Hydroxide Electrode Model

To illustrate the implementation of the control scheme, a two-equation model representing the galvanostatic charge process of a thin film nickel hydroxide electrode<sup>17</sup> is described by the DAE model:

$$\frac{\rho V}{W} \frac{dy(t)}{dt} = \frac{j_1}{F} \quad [11]$$

$$j_1 + j_2 - \alpha I_{app} = 0 \quad [12]$$

$$j_1 = i_{01} \left[ 2(1 - y(t)) \exp\left(\frac{(z(t) - \phi_1)F}{2RT}\right) - 2y(t) \exp\left(-\frac{(z(t) - \phi_1)F}{2RT}\right) \right] \quad [13]$$

$$j_2 = i_{02} \left[ \exp\left(\frac{(z(t) - \phi_2)F}{RT}\right) - \exp\left(-\frac{(z(t) - \phi_2)F}{RT}\right) \right] \quad [14]$$

where the dependent variable  $y$  represents the mole fraction of nickel hydroxide and  $z$  represents the potential difference at the solid-liquid interface. The parameters used in the model Eqs. 11–14 are in listed in Table II.

**Control objective.**—The control objective is defined as a setpoint tracking problem. According to the control objective, an optimal

current density profile is computed that drives the mole fraction (the controlled variable) from its initial state to the desired setpoint. While fulfilling the objective, the bounds are simultaneously imposed on the current density.

The defined control objective can be formulated as the NLP (for scalar  $y$ ):

**Formulation—III:**

$$\min_{I_{app}} \sum_{k=1}^p (y(k) - y^{set})^2 \quad [15]$$

subject to the constraints: model differential and algebraic Eqs. 11–14

$$0 \leq I_{app}(k) \leq I_{app}^{\max}, k = 1, \dots, p \quad [16]$$

- Equation 15 is the setpoint tracking control objective where  $y(k)$  denotes the nickel hydroxide mole fraction for all  $k$  sampling instants over the prediction horizon  $p$ , with each sampling instant of time  $\Delta t$ , and  $y^{set}$  denotes the desired set point for the nickel hydroxide mole fraction.

- Equation 16 defines the bounds on applied current density ( $I_{app}$ ) over the prediction horizon  $p$ , and  $I_{app}^{\max}$  denotes the upper bound on the applied current density.

**Simulation results.**—The NLP Formulation III is solved using NMPC algorithm discussed in Table I. The closed-loop trajectories of nickel hydroxide mole fraction, potential difference at the solid-liquid interface, and applied current density are shown in Fig. 3. The controller tracks the nickel hydroxide mole fraction (controlled variable) to a set point at 0.9. This case study used  $Q = 1$  and  $R = 0$ , and  $I_{app}^{\max} = \{2, 3\}$  A cm<sup>-2</sup> was considered to account physical dissimilarities between different charging units. For satisfying this control objective, the controller is designed with a prediction horizon  $p$  of 3 sampling periods, control horizon  $m$  of 3 sampling periods, and sampling period  $\Delta t$  of 100 s. To study the robustness of the controller, model-plant mismatch is introduced by increasing the mass of the active material  $W$  by 10% in the plant simulation.

The controller validates the observation that a higher maximum input current density results in the mole fraction of the nickel hydroxide electrode reaching its reference value more quickly than for a lower maximum current density.

Bounds on additional state variables (such as voltage ( $z$ ) in this example) can also be introduced in the NMPC framework. Such bounds will be illustrated in detail in the next section, where the implementation of the NMPC strategy using the pseudo-2-dimensional (P2D) model of a lithium-ion battery is discussed.

**Table II. Parameters of the thin-film nickel hydroxide model.**

Symbol	Parameter	Value	Units
$F$	Faraday constant	96,487	C/mol
$R$	Gas constant	8.314	J/mol-K
$T$	Temperature	303.15	K
$\phi_1$	Equilibrium potential	0.420	V
$\phi_2$	Equilibrium potential	0.303	V
$W$	Mass of active material	92.7	g
$V$	Volume	$1 \times 10^{-5}$	m <sup>3</sup>
$i_{01}$	Exchange current density	$1 \times 10^{-4}$	A cm <sup>-2</sup>
$i_{02}$	Exchange current density	$1 \times 10^{-10}$	A cm <sup>-2</sup>
$I_1$	Scaling factor for applied current density	$1 \times 10^{-5}$	unitless
$\rho$	Density	3.4	g cm <sup>-3</sup>

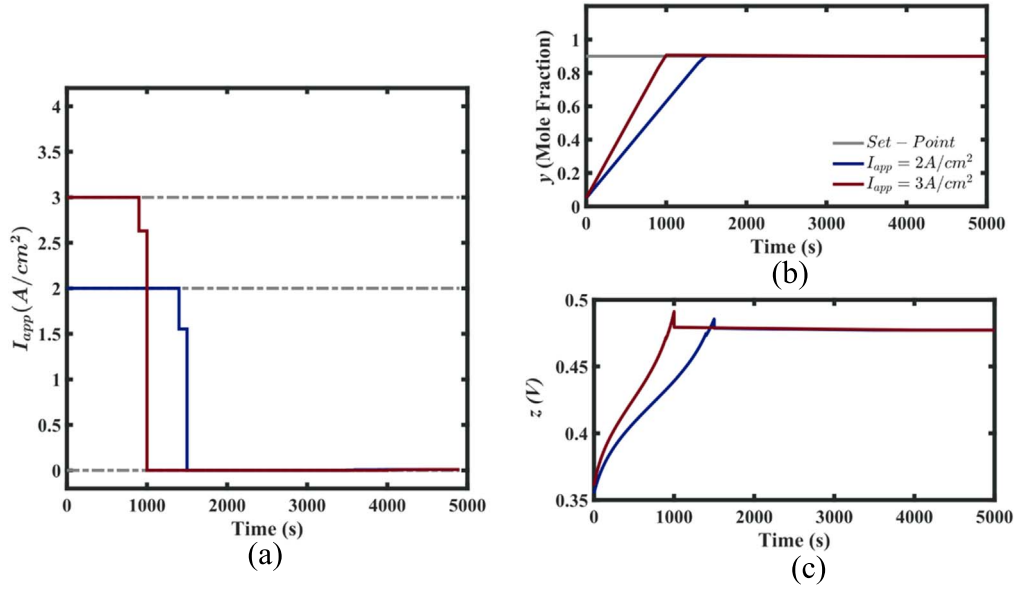


**Figure 3.** NMPC time profiles from Formulation III for (a) current density, (b) mole fraction, and (c) potential. The simulations are performed using “ode15s” from the MATLAB solver suite as the DAE solver and “fmincon sqp” as the NLP solver.

### Pseudo 2-Dimensional (P2D) Model of a Lithium-Ion Battery

The Pseudo-Two-Dimensional (P2D) model is one of the most widely used physics-based electrochemical models for lithium-ion batteries.<sup>18</sup> The complete set of partial differential algebraic equations (PDAEs) describing the governing equations of the P2D model are given in Table AI in the Appendix. The associated expressions and parameters characterizing the model are listed in Tables AII and AIII in the Appendix, respectively. The state variables of the P2D model are:

- $c_p^s, c_n^s$ : Solid-phase lithium concentration in the positive electrode and the negative electrode of the battery
- $\Phi_1$ : Solid-phase potential in both the positive and the negative electrode
- $\Phi_2$ : Electrolyte potential in the positive electrode, negative electrode, and separator.
- $c$ : Lithium-ion concentration in the electrolyte phase across the positive electrode, separator, and negative electrode

Assuming the battery to be limited by the anode capacity, the bulk SOC is calculated as the average of the volume-averaged solid-phase lithium concentration across the negative electrode:

$$SOC(t) = 100 * \left( \frac{\left( \frac{1}{L_n c_s^{\max, n}} \int_0^{L_n} c_s^{avg}(x, t) dx \right) - \theta_{\min}}{\theta_{\max} - \theta_{\min}} \right), \quad [17]$$

where  $c_s^{\max, n}$  denotes the maximum solid-phase concentration of lithium in the negative electrode,  $c_s^{avg}$  denotes the volume-averaged solid-phase concentration in each solid particle in the negative electrode, and  $L_n$  denotes the length of the negative electrode of the battery.  $\theta_{\min}$  and  $\theta_{\max}$  are states of charge at fully discharged and charged states, that depend on the stoichiometric limits of the negative electrode. This choice of controlled variable illustrates the ability and speed of the NMPC algorithm. In general, the batteries are often limited by the lithium concentration in the positive electrode (cathode). Additionally, state variables such as cell voltage or temperature can also be used as controlled variables, as they can be measured directly.

Apart from the main reaction of lithium-ion intercalation, various side reactions occur during charging which may potentially damage the battery.<sup>9,19,20</sup> For example, anodic side reactions may deposit lithium on the surface of the negative electrode (lithium plating) thereby resulting in the subsequent loss of the battery’s capacity.<sup>20,21</sup> The lithium plating occurs when the over-potential at the anode becomes negative.<sup>21</sup> As the open-circuit potential of the lithium plating side reaction is taken as 0 V (vs Li/Li+), the over-potential of the lithium plating side-reaction is defined as

$$\eta_{plating}(x, t) = \Phi_1(x, t) - \Phi_2(x, t) \quad [18]$$

It has been previously shown that lithium plating is more likely to occur at the anode-separator interface at high charging rates<sup>19</sup>; hence we apply constraints only at the anode-separator interface throughout our analysis. As  $\Phi_1$  and  $\Phi_2$  are obtained as internal states of the P2D model, the anode over-potential can be tracked at any time during charging. By constraining the anode over-potential to be non-negative during charging, it is possible to restrict lithium plating side reaction, thereby mitigating battery degradation. The accuracy of the underlying model plays a vital role in predicting and thereby restricting the anode over-potential, as it cannot be directly measured.<sup>20</sup> Therefore, using a detailed physics-based model (P2D model) for BMS helps in minimizing battery degradation, thereby enabling the utilization of the battery to its full potential.

**Control objective.**—The control objective of the proposed NMPC strategy for the P2D model is defined by

$$\varphi = \sum_{k=1}^p (v_k - v^{set})^T Q (v_k - v^{set}) + \sum_{k=1}^m (I_{app,k} - I_{app,k-1})^T R (I_{app,k} - I_{app,k-1}) \quad [19]$$

where  $v_k$  denotes the controlled variable at the time instant  $t_k$ , in which the controlled variable is either SOC or voltage for the system considered;  $v^{set}$  denotes the desired set point for SOC or voltage; and  $I_{app,k}$  denotes the predicted optimal applied current density (input variable) at the time instant  $t_k$ . The first term in Eq. 19 describes the setpoint tracking objective and the second term represents the changes in the applied current density. The weighting factor ( $Q$ )

for setpoint tracking is described by a scalar, due to the presence of a single controlled variable in the electrochemical system under study but can be a vector if there are multiple controlled variables.

For Li-ion batteries, the defined objective can be interpreted as deriving a charge current profile that drives and maintains the controlled variable at a desired operating condition. In doing so, it is desired to simultaneously enforce physical and operational constraints for the safe and optimal charging of a battery. With SOC as the desired controlled variable, the control objective (Eq. 19) is reformulated as the NLP with specific constraints, to obtain the optimal control problem ( $I_{app}^*$ ) with  $Q$  and  $R$  are set as 1 and 0, respectively. The original governing PDAEs are spatially discretized using the strategy described in Northrop et al.<sup>22</sup> and the resulting DAEs of the reformulated P2D model are used as constraints. The convergence analysis on the spatial discretization strategy is discussed in Appendix.

The objective defined in Eq. 19 can also be viewed as a *pseudo minimum charging time* problem as it brings similar results compared to a battery fast-charge problem (a battery fast-charge problem is defined as finding the optimal charging strategy to charge a battery from an initial SOC to the desired SOC, in the shortest possible time, with given constraints on the voltage, current, temperature, overpotential, or other variables, for the same sample time).

Below is a discussion of the derivation of control profiles for various constraints employed on cell voltage and overpotential at the anode-separator interface. Model-plant mismatch and corresponding uncertainty in the model are introduced by changing the parameter

values as shown in the Appendix. The tuning parameters and the bounds used are

$$\begin{aligned} Q &= 1, R = 0, SOC^{set} = 100, V_{LB} = 2.8 \text{ V}, \\ V_{UB} &= 4.2 \text{ V}, I_{app}^{max} = 63 \text{ A m}^{-2}, \\ p &= 4, m = 1, \Delta t = 30 \text{ s} \end{aligned}$$

#### Formulation—IV:

$$\min_{I_{app}^*} \sum_{k=1}^p (SOC_k - SOC^{set})^2 \quad [20]$$

Subject to

$$\text{DAEs Describing the reformulated P2D model} \quad [21]$$

$$V_{LB} \leq V_{cell}(k) \leq V_{UB}, k = 1, \dots, p \quad [22]$$

$$0 \leq I_{app}^*(k) \leq I_{app}^{max}, k = 1, \dots, p \quad [23]$$

- The objective function in Eq. 20 is the minimization of the normed distance between SOC and its setpoint  $SOC^{set}$ .

- Equation 21 are the set of DAEs obtained in the reformulated model after spatially discretizing the governing PDAEs given in the Table AI.<sup>18</sup>

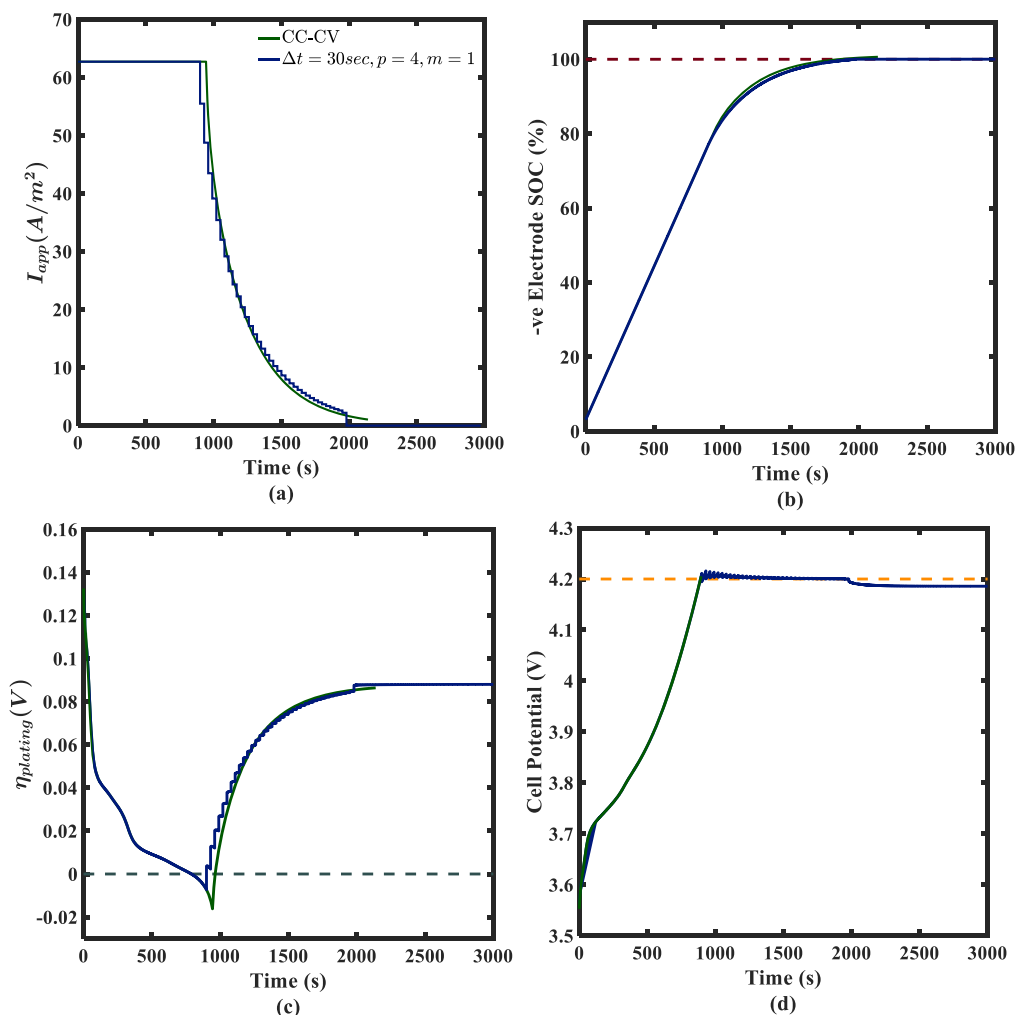


Figure 4. Comparison of model simulation at CC-CV (green) and NMPC strategy (blue) with out constraint on over-potential.

• Equation 22 represents bounds on the overall cell voltage. Imposing bounds on the overall voltage of the battery is essential for its safe operation. Every battery is rated by the battery manufacturer to be operated within a specified voltage window. Hence, for safety (and legal warranty issues imposed by the battery manufacturer in most cases), it is recommended to restrict the battery voltage within a finite window described by (22).

• Equation 23 describes the bounds on the applied current density over the prediction horizon  $p$ .

This study considers an isothermal model to demonstrate the methodology and the computational time of the algorithm. However, additional constraints on other state variables such as temperature can also be included in the algorithm using a thermal model.

Figure 4 shows the comparison between traditional CC-CV profiles and optimal control profiles obtained using Formulation IV. NMPC strategy drives and maintains the SOC at its setpoint of 100% while enforcing the bounds on the applied current density and cell voltage. Once the SOC reaches its setpoint, the controller progressively drops current density to zero as expected, thereby maintaining the desired setpoint conditions. This results in a control profile that qualitatively follows the traditional CC-CV profile until the desired SOC is reached, while essentially charging a battery to the final SOC in the shortest possible time. However, it should be noted that the overpotential for the lithium plating reaction at the anode-separator interface becomes negative ( $\eta_{\text{plating}} < 0$ ) at a certain time while charging. As discussed before, this behavior while charging might lead to the deposition of lithium on the surface of the negative electrode, leading to capacity fade and dendrite

formation. Therefore, for ensuring safe operating conditions, constraints are imposed on the plating overpotential to avoid the regimes where  $\eta_{\text{plating}} < 0$ , as in Formulation V.

**Formulation—V:**

$$\min_{I_{app}} \sum_{k=1}^p (SOC_k - SOC^{set})^2 \quad [24]$$

Subject to

$$\text{DAEs Describing the reformulated P2D model} \quad [25]$$

$$V_{LB} \leq V_{cell}(k) \leq V_{UB}, k = 1, \dots, p \quad [26]$$

$$0 \leq I_{app}^*(k) \leq I_{app}^{\max}, k = 1, \dots, p \quad [27]$$

$$\eta_{\text{plating}} = \Phi_1(k) - \Phi_2(k) > 0, k = 1, \dots, p \quad [28]$$

In addition to the constraints described in Formulation IV, Eq. 28 describes the constraints on the lithium plating overpotential over the predictive horizon  $p$ . As previously discussed, this constraint mitigates battery degradation due to lithium plating.

Figure 5 shows the comparison of the traditional CC-CV profiles and optimal control profiles obtained after adding the constraints on overpotential. The results in this case study show that the proposed manipulated variable profiles drive the controlled variable to a desired set point, in the least time possible, while enforcing

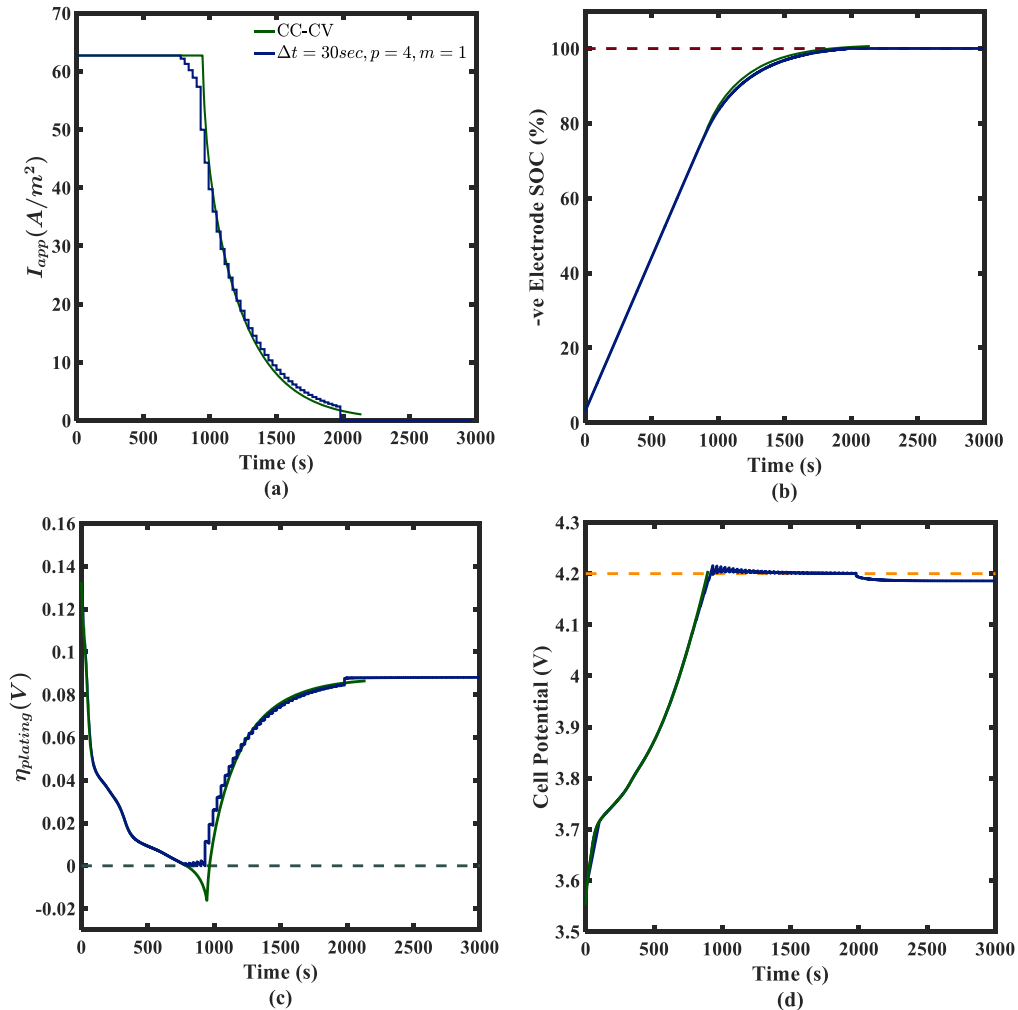


**Figure 5.** Comparison of model simulation at CC-CV (green) and NMPC strategy (blue) with constraint on over-potential.

constraints on the mechanisms which degrade the battery life. Achieving the same SOC levels using a conventional CC-CV charging profile will lead to negative side overpotential which might potentially degrade the battery performance. In other words, though conventional CC-CV protocols are time tested, the significance of optimal control profiles can be gauged when NMPC strategies are implemented while experimentally cycling the cells.

**Servo problem.**—The explicit time dependence of the stage cost/control objective and equality and inequality constraints (comprising model equation constraints, input, and state variable constraints) allow for the incorporation of dynamic setpoint trajectories in NLP defined by (5)–(9).<sup>15</sup> In certain applications, it may be desirable for the batteries to experience specific dynamic voltage profiles. Here, NMPC results are presented for a time-varying setpoint on the voltage.

**Formulation—VI:**

$$\min_{I_{app}} \sum_{k=1}^p (V_k - V^{set})^2 \quad [29]$$

Subject to

$$V_{LB} \leq V_{cell}(k) \leq V_{UB}, k = 1, \dots, p \quad [30]$$

$$0 \leq I_{app}^*(k) \leq I_{app}^{max}, k = 1, \dots, p \quad [31]$$

$$\eta_{plating} = \Phi_1(k) - \Phi_2(k) > 0, k = 1, \dots, p \quad [32]$$

where  $V^{set}$  is given by the “red” dashed line in Fig. 6d. The controller, in this case, was designed with  $p = 3$ ,  $m = 2$ , and  $\Delta t = 30$  s. Figure 6 shows the control profiles obtained for a dynamic setpoint trajectory.

**Computational Details**

Traditionally, the incorporation of a detailed physics-based model (P2D model) in BMS applications has been said to be computationally expensive due to their large simulation times.<sup>7</sup> Therefore, incorporation of such models for real-time simulation and control applications necessitates efficient, fail-proof and fast solvers. In our previous work, we demonstrated the simulation of the reformulated P2D model with computation time of 15 to 100 ms.<sup>20,22–24</sup> This reduction in the simulation time facilitates the use of P2D model for real-time control applications using NMPC, as demonstrated by the results obtained from this work. All the results reported in this work are obtained using MATLAB. In this environment, the single optimization call to identify optimal current density for single prediction horizon using detailed P2D model was approximately 60 s. The detailed summary of the computation time (using MATLAB) for all cases is given in Table III. The computational time (including single optimization call and single model simulation call) for the NMPC strategy with P2D model will be

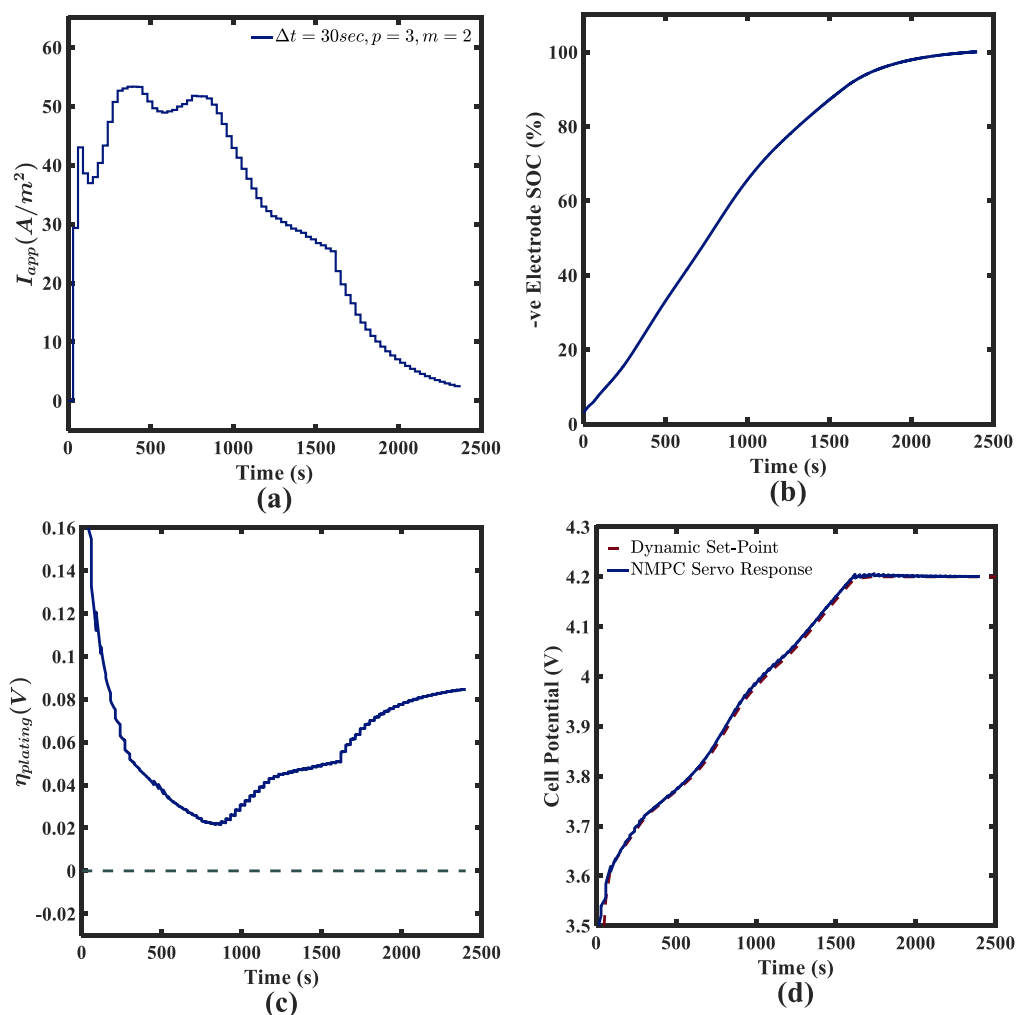


**Figure 6.** NMPC time profiles for Formulation VI to identify optimal current density required to match dynamically varying set-points on cell potential.



**Table III. Summary of the Formulations.**

Formulation		Formulation Description		
Formulation	Case Study	In MATLAB Single Optimization Call (s)	Single Simulation Call (s)	Remarks
I				Generic optimal control problem in NMPC framework in a continuous form
II				The generic optimal control formulation through discretization of the continuous input signal of the NMPC framework into a set of finite number of control parameters
III	Thin-Film Electrode	≈1	≈0.0088	A simple example showing implementation of NMPC framework with bounds on applied current density using sequential approach.
IV	Isothermal P2D	≈45	≈0.8	Implementation of NMPC strategy without any constraints on over-potential. The bounds are specified on cell potential and manipulated variable, current density ( $I_{app}$ ).
V	Isothermal P2D	≈55	≈0.8	Included constraints on over-potential in Formulation—IV. Compared to Formulation—IV, there is change in current density profile to avoid lithium plating. The optimal control profiles is close to conventional CC-CV charging protocol. But optimal charging is always better strategy as it has the ability to avoid over charging as well as plating compared to conventional charging.
VI	Isothermal P2D	≈65	≈0.66	In control theory, it is a servo problem. In practice, some of the applications can have dynamic cell potential profiles. This case studies the ability to implement NMPC strategies that manipulate current density to match dynamic set-points.

lower ( $\approx 2$  s) when deployed in the C environment. The obtained computational efficiency demonstrates that a detailed P2D model can be used for real-time control applications of BMS. Such detailed models facilitate aggressive and optimal charging protocols, thereby extracting maximum performance from the cell.

**Note.**—The robustness of this sequential approach relies on the integration solver (odes15s in MATLAB or IDA in C) used in the nonlinear programming problems. In general, the isothermal and thermal battery models pioneered by John Newman are index-1 DAE's. ODE15s is numerical integrator in MATLAB that can handle only index-1 DAEs. There are more robust solvers for index-1 DAE's such as IDA in C developed by SUNDIALs or DASSL/DASSPL.<sup>25</sup> If pressure models are considered in addition to electrochemical models, the resulting DAE's are index-2 DAEs.<sup>26</sup> The best solvers for index-2 DAEs are RADAU.<sup>27</sup> The use of these solver requires the specification of exact initial conditions for the algebraic variables and also requires the identification of index 2 variables.

As of today, for higher index DAEs, the best option is to reformulate and reduce these DAEs to index-1 DAEs and then solve them using Pantelides Algorithm. The difficulty for higher index DAEs are limited to sequential approach. Even for simultaneous approach, there will be reduction in accuracy for higher index DAEs.

### Summary

This article presents implementation of nonlinear model predictive control on physics-based battery models for deriving optimal charging protocols. We have shown that the designed NMPC controller is efficient in satisfying the given control objectives in the presence of different constraints on the internal state variable and applied current density. It is shown that the proposed controller, through constraining the plating overpotential, can efficiently derive health-conscious charging profiles while still charging the battery to the desired setpoint on SOC. Further, the effectiveness of the controller in tracking a dynamically varying setpoint is also demonstrated. This study demonstrates that a detailed P2D model can be incorporated in the design of ABMS for enabling real-time control of Li-ion batteries. While the objective has been formulated as set-point based on SOC or cell voltage, it can easily be modified to minimize the capacity fade over a charging period (provided that the capacity fade model is incorporated) or minimize the total charging time with constraints on the total charge stored, among others. The formulations discussed in this work are summarized in Table III.

For future investigations, we plan to explore implementation of simultaneous numerical optimization strategies instead of sequential strategies for solving the NMPC optimal control problems. Simultaneous strategies, apart from being computationally less expensive, do not depend on a robust DAE solver for evaluating the objective and constraint functions. Further, path constraints through simultaneous strategy can be handled in a more efficient way and need not be approximated as with sequential approach. However, this requires careful and sufficient discretization strategies in time (number of elements, method of discretization, etc.) which will be reported in the future. Future publications will also report on the implementation of an output feedback NMPC, where a nonlinear state estimator is incorporated in the existing framework, for providing the full state information at each sampling instant.

### Acknowledgments

The authors would like to thank the U.S. Department of Energy (DOE) for providing partial financial support for this work, through the Advanced Research Projects Agency (ARPA-E) award number DE-AR0000275. The work at University of Texas at Austin was also partially supported by DOE award DEAC05-76RL01830 through PNNL subcontract 475525. The authors would like to express gratitude to Assistant Secretary for Energy Efficiency and Renewable Energy, Office of Vehicle Technologies of the DOE through the Advanced Battery Material Research (BMR) Program (Battery500 consortium).

### Appendix

**Numerical procedure.**—The governing equations and boundary conditions of the P2D model given in Table AI are a set of partial differential equations (PDAEs). The additional expressions and parameters are given in Table AII and Table AIII, respectively. These PDAEs in each region are discretized using the coordinate transformation and orthogonal collocation (OC) proposed by Northrop et al.,<sup>22</sup> The convergence analysis for OC = {1, 2, 3, 4, 5} points in each region are performed for 3C charge rate and the comparisons are shown in Fig. A1. The Fig. A1 shows the convergence analysis for (a) overall cell potential, (b) temporal plot of the overpotential at the negative electrode—separator interface and (c) the spatial variation of the electrolyte concentration across the three regions of the cell. Throughout this work in Formulations IV–VI, OC = 3 points are taken to discretize the PDAEs that results in spatially and temporally converged profiles for

**Table AI. Governing PDEs for the P2D model.**

Governing Equations	Boundary Conditions
<p><b>Positive Electrode</b></p> $\varepsilon_p \frac{\partial c}{\partial t} = \frac{\partial}{\partial x} \left[ D_{eff,p} \frac{\partial c}{\partial x} \right] + a_p (1 - t_+) j_p$ $i_2 = -\kappa_{eff,p} \frac{\partial \Phi_2}{\partial x} + \frac{2\kappa_{eff,p} RT}{F} (1 - t_+) \left( 1 + \frac{\partial \ln f}{\partial \ln c} \right) \frac{1}{c} \frac{\partial c}{\partial x}$ $\frac{\partial}{\partial x} \left[ \sigma_{eff,p} \frac{\partial \Phi_1}{\partial x} \right] = a_p F j_p$ $\frac{\partial c_p^s}{\partial t} = \frac{1}{r^2} \frac{\partial}{\partial r} \left[ r^2 D_p^s \frac{\partial c_p^s}{\partial r} \right]$	$\frac{\partial c}{\partial x} \Big _{x=0} = 0$ $-D_{eff,p} \frac{\partial c}{\partial x} \Big _{x=l_p^-} = -D_{eff,s} \frac{\partial c}{\partial x} \Big _{x=l_p^+}$ $\frac{\partial \Phi_2}{\partial x} \Big _{x=0} = 0$ $-\kappa_{eff,p} \frac{\partial \Phi_2}{\partial x} \Big _{x=l_p^-} = -\kappa_{eff,s} \frac{\partial \Phi_2}{\partial x} \Big _{x=l_p^+}$ $\frac{\partial \Phi_1}{\partial x} \Big _{x=0} = -\frac{I_{app}}{\sigma_{eff,p}}$ $\frac{\partial \Phi_1}{\partial x} \Big _{x=l_p^-} = 0$ $\frac{\partial c_p^s}{\partial r} \Big _{r=0} = 0$ $\frac{\partial c_p^s}{\partial r} \Big _{r=R_p} = -\frac{j_p}{D_p^s}$

Table AI. (Continued).

Governing Equations	Boundary Conditions
<b>Separator</b>	
$\varepsilon_s \frac{\partial c}{\partial t} = \frac{\partial}{\partial x} \left[ D_{eff,s} \frac{\partial c}{\partial x} \right]$	$c _{x=l_p^-} = c _{x=l_p^+}$
$i_2 = -\kappa_{eff,s} \frac{\partial \Phi_2}{\partial x} + \frac{2\kappa_{eff,s}RT}{F}(1-t_+) \left( 1 + \frac{\partial \ln f}{\partial \ln c} \right) \frac{1}{c} \frac{\partial c}{\partial x}$	$c _{x=l_p+l_s^-} = c _{x=l_p^+ + l_s^+}$
<b>Negative electrode</b>	
$\varepsilon_n \frac{\partial c}{\partial t} = \frac{\partial}{\partial x} \left[ D_{eff,n} \frac{\partial c}{\partial x} \right] + a_n(1-t_+)j_n$	$\frac{\partial c}{\partial x} \Big _{x=l_p+l_s+l_n} = 0$
$i_2 = -\kappa_{eff,n} \frac{\partial \Phi_2}{\partial x} + \frac{2\kappa_{eff,n}RT}{F}(1-t_+) \left( 1 + \frac{\partial \ln f}{\partial \ln c} \right) \frac{1}{c} \frac{\partial c}{\partial x}$	$-D_{eff,s} \frac{\partial c}{\partial x} \Big _{x=l_p+l_s^-} = -D_{eff,n} \frac{\partial c}{\partial x} \Big _{x=l_p+l_s^+}$
$\frac{\partial}{\partial x} \left[ \sigma_{eff,n} \frac{\partial \Phi_1}{\partial x} \right] = a_n F j_n$	$\Phi_2 _{x=l_p+l_s+l_n} = 0$
$\frac{\partial c_n^s}{\partial t} = \frac{1}{r^2} \frac{\partial}{\partial r} \left[ r^2 D_n^s \frac{\partial c_n^s}{\partial r} \right]$	$-\kappa_{eff,s} \frac{\partial \Phi_2}{\partial x} \Big _{x=l_p+l_s^-} = -\kappa_{eff,p} \frac{\partial \Phi_2}{\partial x} \Big _{x=l_p+l_s^+}$
	$\frac{\partial \Phi_1}{\partial x} \Big _{x=l_p+l_s^-} = 0$
	$\frac{\partial \Phi_1}{\partial x} \Big _{x=l_p+l_s+l_n} = -\frac{l_{app}}{\sigma_{eff,n}}$
	$\frac{\partial c_n^s}{\partial r} \Big _{r=0} = 0$
	$\frac{\partial c_n^s}{\partial r} \Big _{r=R_n} = -\frac{j_n}{D_n^s}$

Table AII. Additional expressions used in the P2D model.

$$j_p = 2k_p c^{0.5} c_s^{0.5} \Big|_{r=R_p} (c_{max,p}^s - c^s|_{r=R_p})^{0.5} \times \sinh \left[ \frac{F}{2RT} (\Phi_1 - \Phi_2 - U_p) \right]$$

$$j_n = 2k_n c^{0.5} c_s^{0.5} \Big|_{r=R_n} (c_{max,n}^s - c^s|_{r=R_n})^{0.5} \times \sinh \left[ \frac{F}{2RT} (\Phi_1 - \Phi_2 - U_n) \right]$$

$$\kappa_{eff,i} = \varepsilon_i^{brugsi} \left( \begin{array}{l} 1 \times 10^{-4} c ((-10.5 + 0.0740T - 6.96 \times 10^{-5} T^2)) \\ + 0.001 c (0.668 - 0.0178T + 2.8 \times 10^{-5} T^2) \\ + 1 \times 10^{-6} c^2 (0.494 - 8.86 \times 10^{-4} T)^2 \end{array} \right)$$

$$i = p, s, n$$

$$\sigma_{eff,i} = \sigma_i (1 - \varepsilon_i - \varepsilon_{f,i}), i = p, s, n$$

$$D_{eff,i} = D \varepsilon_i^{brugsi}, i = p, s, n$$

$$D = 0.0001 \times 10^{-4.43 - 54(T - 229 - 0.005c)^{-1} - 0.00022c}$$

$$a_i = \frac{3}{R_i} (1 - \varepsilon_i - \varepsilon_{f,i}), i = p, s, n$$

$$U_p = -10.72\theta_p^4 + 23.88\theta_p^3 - 16.77\theta_p^2 + 2.595\theta_p + 4.563$$

$$\theta_p = \frac{c^s|_{r=R_p}}{c_{max,p}^s}$$

$$U_n = 0.1493 + 0.8493e^{-61.79\theta_n} + 0.3824e^{-665.8\theta_n} - e^{39.42\theta_n - 41.92} - 0.03131 \tan^{-1}(25.59\theta_n - 4.099) - 0.009434 \tan^{-1}(32.49\theta_n - 15.74)$$

$$\theta_n = \frac{c^s|_{r=R_n}}{c_{max,n}^s}$$

$$(1 - t_+) \left( 1 + \frac{\partial \ln f}{\partial \ln c_i} \right) = 0.601 - 7.5894 \times 10^{-3} c_i^{0.5} + 3.1053 \times 10^{-5} (2.5236 - 0.0052T) c_i^{1.5}, i = p, s, n$$

Table AIII. Parameters used in the P2D model.

Symbol	Parameter	Positive Electrode	Separator	Negative Electrode	Units
$Brugg$	Bruggeman Coefficient	1.5	1.5	1.5	
$c_{i,max}^s$	Maximum solid phase concentration	51830		31080	mol/m <sup>3</sup>
$c_{i,0}^s$	Initial solid-phase concentration	18646		24578	mol/m <sup>3</sup>
$c_0$	Initial electrolyte concentration	1200	1200	1200	mol/m <sup>3</sup>
$D_i^s$	Solid-phase diffusivity	2e-14		1.5e-14	m <sup>2</sup> /s
$F$	Faraday's constant		96487		C/mol
$k_i$	Reaction rate constant	6.3066e-10		6.3466e-10	m <sup>2.5</sup> /(mol <sup>0.5</sup> s)
$l_i$	Region thickness	41.6e-6	25e-6	48e-6	m
$R_{p,i}$	Particle Radius	7.5e-6		10e-6	m
$R$	Gas Constant		8.314		J/(molK)
$T$	Temperature		298.15		K
$t_+$	Transference number		0.38		
$\epsilon_{f,i}$	Filler fraction	0.12		0.038	
$\epsilon_i$	Porosity	0.3	0.4	0.3	
$\sigma_i$	Solid-phase conductivity	100		100	S/m

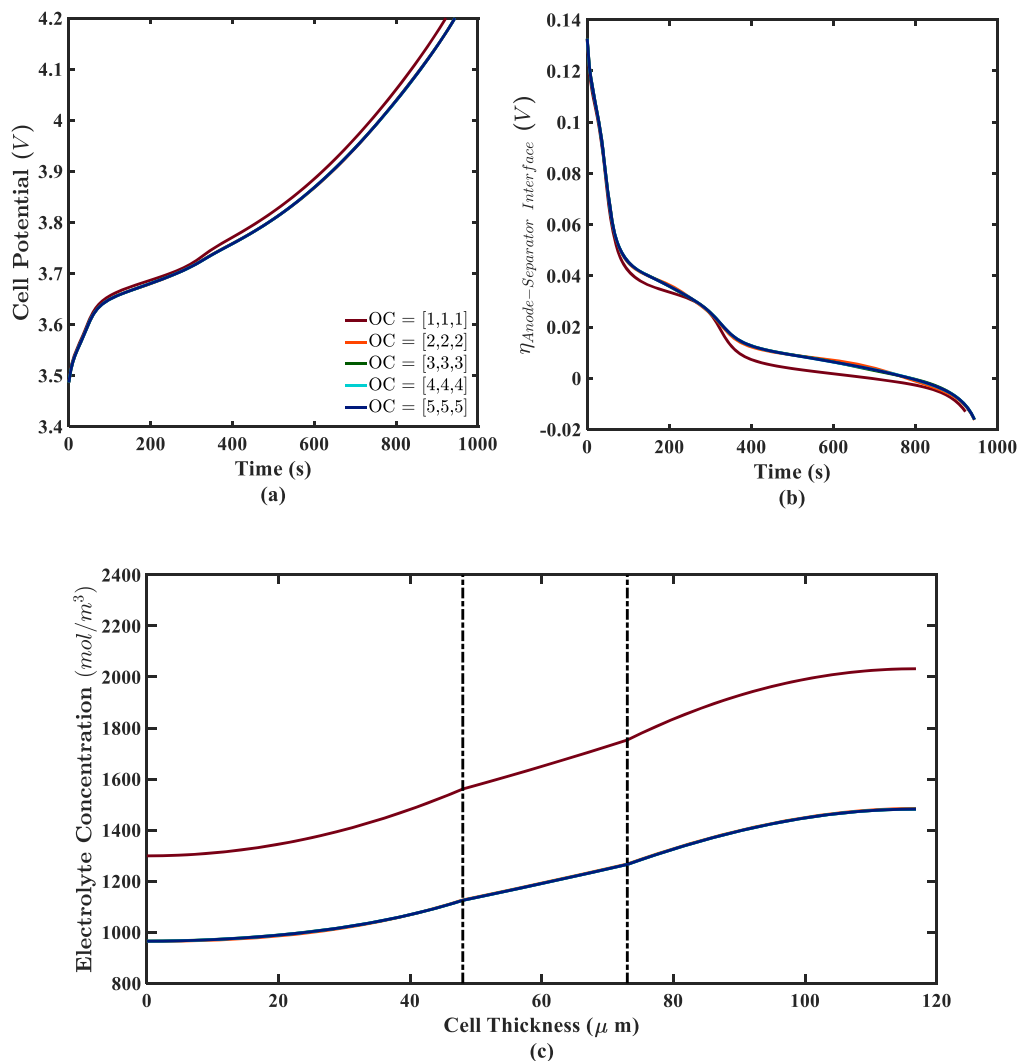
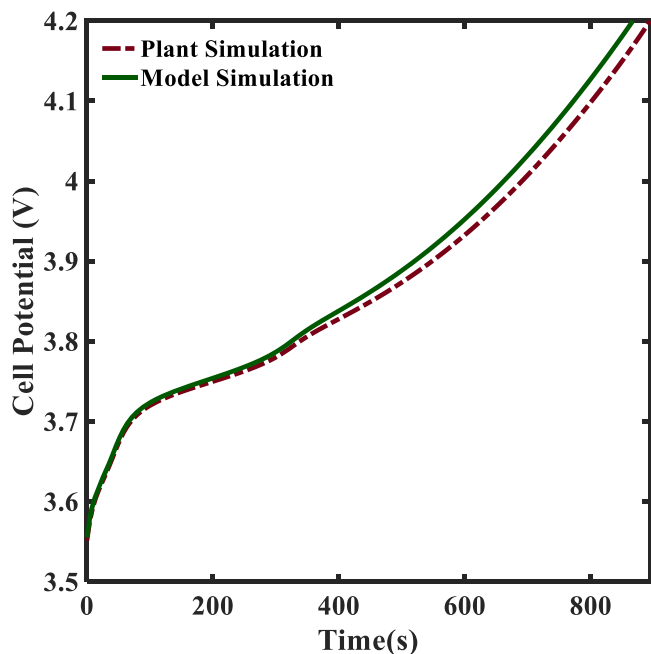


Figure A1. Convergence analysis of the P2D model discretized using co-ordinate transformation and orthogonal collocation. The analysis performed for (a) overall cell potential, (b) overpotential at the anode—separator interface and (c) spatial variation of the electrolyte concentration across the three regions of the cell at 3C charge simulation.



**Figure A2.** Model uncertainty introduced by changing the solid-phase diffusivity and conductivity kinetic rate constant of the positive electrode as mentioned in Table A IV (a) Model simulation (green line), (b) Plant simulation (red dotted).

**Table AIV. Parameters used for plant and model simulations.**

Parameter Values	Plant	Model
$D_p^s$	2e-14	2.4e-14
$k_p$	6.3066e-10	7.567e-10


all internal variables, with less than 10 mV error in the voltage vs time curve (Plots for OC > [3, 3, 3] lie on top of each other).

**Model Uncertainty (Model-Plant mismatch).**—For this work, the plant is simulated by the same model equations. Uncertainty in the model (signifying error in the model), and a corresponding mismatch with the plant, is introduced by perturbing the model parameters compared to the plant parameters. Figure A2 shows the

comparison of model vs plant dynamics for a simulation performed at 3C charge rate, using parameters listed in Table AIV.

#### ORCID

Suryanarayana Kolluri  <https://orcid.org/0000-0003-2731-7107>

Richard D. Braatz  <https://orcid.org/0000-0003-4304-3484>

Venkat R. Subramanian  <https://orcid.org/0000-0002-2092-9744>

#### References

1. J. Liu, G. Li, and H. K. Fathy, *J. Dyn. Syst. Meas. Control*, **138**, 1 (2016).
2. X. Hu, H. E. Perez, S. J. Moura, H. E. Perez, and S. J. Moura, *Proceedings of the ASME 2015 Dynamic Systems and Control Conference*, **1**, 1 (2015).
3. H. E. Perez, X. Hu, S. Dey, and S. J. Moura, *IEEE Trans. Veh. Technol.*, **66**, 7761 (2017).
4. M. Pathak, D. Sonawane, S. Santhanagopalan, and V. R. Subramanian, *ECS Trans.*, **75**, 51 (2017).
5. M. A. Xavier and M. S. Trimboli, *J. Power Sources*, **285**, 374 (2015).
6. M. Torchio, N. A. Wolff, D. M. Raimondo, L. Magni, U. Kreuer, R. B. Gopaluni, J. A. Paulson, and R. D. Braatz, *Proc. Am. Control Conf.*, **2015**, 4536 (2015).
7. M. Torchio, L. Magni, R. D. Braatz, and D. M. Raimondo, *J. Electrochem. Soc.*, **164**, A949 (2017).
8. M. Torchio, L. Magni, R. D. Braatz, and D. M. Raimondo, *IFAC-PapersOnLine*, **49**, 827 (2016).
9. R. Klein et al., *Proceedings of the 2011 American Control Conference*, Piscataway, NJ(IEEE) p. 382 (2011).
10. J. Lee, P. Zhang, L. K. Gan, D. A. Howey, M. A. Osborne, A. Tosi, and S. Duncan, *IEEE J. Emerg. Sel. Top. Power Electron.*, **6**, 1783 (2018).
11. J. Liu, G. Li, and H. K. Fathy, *IEEE Trans. Control Syst. Technol.*, **25**, 1882 (2017).
12. A. A. Patwardhan, J. B. Rawlings, and T. F. Edgar, *Chem. Eng. Commun.*, **87**, 123 (1990).
13. J. W. Eaton and J. B. Rawlings, *Chem. Eng. Sci.*, **47**, 705 (1992).
14. V. M. Ehlinger and A. Mesbah, *Model Predictive Control of Chemical Processes: A Tutorial*, 367 (2017).
15. M. Huba, S. Skogestad, M. Fikar, M. Hovd, T. A. Johansen, and B. Rohal-Ilkiv, *Selected Topics on Constrained and Nonlinear Control*, 187 (2011).
16. L. T. Biegler, *Nonlinear Programming: Concepts, Algorithms, and Applications to Chemical Processes* (Society of Industrial and Applied Mathematics, Philadelphia, United States of America) p. 416 (2010).
17. B. Wu and R. E. White, *Comput. Chem. Eng.*, **25**, 301 (2001).
18. M. Doyle, T. F. Fuller, and J. Newman, *J. Electrochem. Soc.*, **140**, 1526 (1993).
19. B. Suthar, *Thesis*, Washington University in St. Louis (2015).
20. P. W. C. Northrop, B. Suthar, V. Ramadesigan, S. Santhanagopalan, R. D. Braatz, and V. R. Subramanian, *J. Electrochem. Soc.*, **161**, E3149 (2014).
21. R. Klein, N. A. Chaturvedi, J. Christensen, J. Ahmed, R. Findeisen, and A. Kojic, *Proceedings of the 2010 American Control Conference*, Piscataway, NJ (IEEE) p. 6618 (2010).
22. P. W. C. Northrop, V. Ramadesigan, S. De, and V. R. Subramanian, *J. Electrochem. Soc.*, **158**, A1461 (2011).
23. M. T. Lawder, V. Ramadesigan, B. Suthar, and V. R. Subramanian, *Comput. Chem. Eng.*, **82**, 283 (2015).
24. V. R. Subramanian, V. Boovaragavan, V. Ramadesigan, and M. Arabandi, *J. Electrochem. Soc.*, **156**, A260 (2009).
25. L. R. Petzold, *IMACS World Congress* (Montreal, Canada) (1992).
26. S. De, B. Suthar, D. Rife, G. Sikh, and V. R. Subramanian, *J. Electrochem. Soc.*, **160**, A1675 (2013).
27. E. Hairer and G. Wanner, *Solving Ordinary Differential Equations II, Stiff and Differential-Algebraic Problems*, 72 (1996).